

Accurate quantification of the Purcell effect in the presence of a dielectric microdisk of nanoscale thickness

M.V. Balaban¹, R. Sauleau², T.M. Benson³, A.I. Nosich¹

¹Institute of Radio-Physics and Electronics NASU, Kharkiv 61085, Ukraine

²IETR, Université de Rennes 1, Campus Beaulieu, Rennes 35042, France

³George Green Institute for Electromagnetics Research, University of Nottingham, Nottingham NG7 2RD, UK

E-mail: mikhail.balaban@gmail.com

Published in *Micro & Nano Letters*; Received on 31st January 2011; Revised on 24th May 2011

The spontaneous emission of a molecular dipole in the presence of a thin dielectric microdisk is studied as a 3D solution of Maxwell's equations with two-sided generalised boundary conditions on the disk median plane, local energy finiteness and a radiation condition at infinity. Results presented show that the radiative and non-radiative decay rates display resonance maxima associated with the disk natural frequencies which can be explained through the effective-refractive-index approximation. The numerical solution is based on a set of coupled integral equations of the Fredholm second kind, with smooth kernel functions, obtained with the aid of the method of analytical regularisation.

1. Introduction: The term 'Purcell effect' labels resonant enhancement or, in more a general sense, modification of the spontaneous emission of an atomic or molecular dipole in a non-homogeneous environment [1–3]. Today's interest in this phenomenon is explained by the ability of various nano and micro-size particles to increase spontaneous emission by many orders of magnitude; such enhancement leads directly to applications connected to micro-lasers and cavity quantum electrodynamics. More precisely the study of this effect deals with the radiative and non-radiative decay rates in the presence of resonant particles and their aggregates such as microcavities, photonic molecules and various optical nanoantennas [4–6]. As a rule the Purcell effect has been estimated using the so-called 'Purcell factor' that is proportional to the ratio of the resonant mode quality factor Q to the mode volume V . However, it has been recently convincingly argued that this factor, originally derived for closed cavities with imperfectly conducting walls, cannot be used in the case of open resonators such as noble-metal nanoantennas and semiconductor microdisks. The reasons are 2-fold: here the natural modes do not form a complete orthogonal set of field functions and the resonance does not lead to one-term representation of the spontaneous emission rate [7]. Therefore for an accurate estimation of the Purcell effect for open resonators it is mandatory to use full-wave modelling methods and convergent computational techniques. The aim of this Letter is to present an illustration of such an analysis for a thin disk resonator and to demonstrate that the associated resonances can be explained using the empirical concept of effective refractive index.

Many analytical high-frequency approximations and direct computational methods have been used for the wave scattering analysis in the context of spontaneous emission, optical antennas and various resonance scatterers. In the 3D modelling, the benchmark case is a uniform or concentrically layered material sphere solvable by the separation of variables (Mie theory). If applied to a collection of spheres, the Mie theory leads to infinite-matrix equations with favourable features [8]. For non-separable 3D geometries, accurate computational tools are scarce. Ray-tracing high-frequency methods are physically transparent; however, they fail to reproduce fine details of the wave field and have uncertain domains of applicability. Useful and flexible direct computational methods such as the finite-difference time-domain (FDTD) technique suffer from other problems including boundary staircasing, back-reflections from the computational window, huge-size matrix inversion, and a lack of convergence. As a result, computing a wavelength scan of the emission rate with FDTD is painful. More specifically, FDTD codes can fail to 'see' resonances with $Q \geq 10^5$ unless

very large time intervals are used in the numerical Fourier transformations [9, 10]. Therefore volume and boundary integral equation (IE) methods appear to be more economic and reliable (if properly implemented) tools.

Consider the problem of finding the electromagnetic field emitted by an elementary electric dipole (EED) located at the height h above a material (i.e. magnetodielectric) disk of radius a and thickness τ (Fig. 1). The total field can be viewed as a sum of the incident and scattered fields, the incident field being generated by the same EED in free space. It has to satisfy the inhomogeneous Maxwell equations off the disk surface, the boundary conditions on this surface, and the radiation condition at infinity. For simplicity, we will further consider the case of an EED placed on the axis of rotation and oriented parallel to the disk, although this is not a limitation of the method used. Then the azimuthal dependence of both the incident and the scattered field functions, in the natural cylindrical coordinates (ρ, φ, z) , is $\cos \varphi$ or $\sin \varphi$ depending on the component type, that is its azimuthal order is $m = 1$.

The problem formulated can be reduced to a volume IE in a manner similar to [11]. This is, however, a singular IE whose accurate discretisation is difficult and typically leads to thousands of unknowns even for a nanoscale scatterer. Additionally, the convergence is questionable (especially at the resonances) in the sense that solving progressively larger matrices does not lead to smaller computation errors. As a consequence, the volume IE approach is yet to become a practical tool for a detailed parametric analysis of disk scatterers. The same problem can be also cast to a set of boundary IEs. Although boundary equations lead to more economic discretisations than volume ones, they should be used with great care as many forms of such IEs possess spurious eigenvalues, which spoil the associated numerical algorithms [12]. Even if this is avoided by using Muller's IEs [13], the corresponding algorithms should a priori meet difficulties if applied to the study of thin disks; additionally, the way of handling the edges of the disk cross-section should affect the convergence. All this, together with general difficulty of working with four coupled boundary IEs, has apparently prevented them from being an object of study in 3D analyses; the published results relate to 2D models only [14].

If the disk thickness is small ($\tau \ll \lambda$), as typical for microdisk lasers and nanoparticles, one can build a much more economic algorithm having guaranteed convergence. The foundations of this approach and basic equations can be found in [15]; its implementation for an arbitrarily located dipole will be the subject of a separate publication. The initial step is to simplify the problem by neglecting the field inside the disk and shrinking

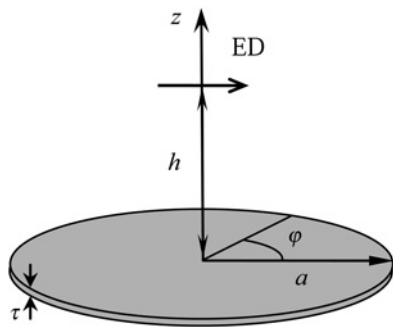


Figure 1 Geometry of a dipole above a dielectric microdisk

the disk volume to the median section, at the expense of introducing two-sided generalised boundary conditions (GBCs) at that section [16]

$$\begin{aligned} (\mathbf{E}_{\text{tg}}^+ + \mathbf{E}_{\text{tg}}^-) &= 2Z_0 R \cdot \mathbf{n} \times (\mathbf{H}_{\text{tg}}^+ - \mathbf{H}_{\text{tg}}^-) \\ (\mathbf{H}_{\text{tg}}^+ + \mathbf{H}_{\text{tg}}^-) &= -2Z_0^{-1} Q \cdot \mathbf{n} \times (\mathbf{E}_{\text{tg}}^+ + \mathbf{E}_{\text{tg}}^-) \end{aligned} \quad (1)$$

Here, Z_0 is the free-space impedance, R and Q are the relative electric and magnetic resistivities, \mathbf{n} is the one-side unit normal vector, and the subscript tg marks the tangential field vectors. In the case of the material of the disk being optically dense ($|\varepsilon_r \mu_r| \gg 1$), one finds that [16]

$$R = iZ/2 \cdot \cot(\sqrt{\varepsilon_r \mu_r} k \tau / 2), \quad Q = i/(2Z) \cdot \cot(\sqrt{\varepsilon_r \mu_r} k \tau / 2) \quad (2)$$

where $k = \omega/c = 2\pi/\lambda$ is the wavenumber, $Z = \sqrt{\mu_r/\varepsilon_r}$ is the relative impedance, and ε_r and μ_r are the relative permittivity and permeability of the disk material, respectively. Note that the error incurred in replacing the disk with GBCs can be accurately found only if confronted with an accurate ‘thick-disk’ solution. Unfortunately, the latter solution is currently not available on a sufficiently large domain of variation of the wavelength, disk thickness and other parameters, apparently for the reasons discussed above. A partial justification, however, has been done in the similar GBC-based analysis of dielectric-strip gratings [17] using the volume IE solution as a reference.

Further we present the field components in terms of a Fourier series in the azimuthal coordinate φ and scalar and vector Hankel integral transforms in the radial coordinate [15]. Substituting these functions into the GBCs, we obtain a set of dual IEs for each azimuthal order m . Then we use the method of analytical regularisation (see [18] for a review of this approach) to invert their static parts and reduce them to two pairs of coupled Fredholm second kind IEs with smooth kernels. This procedure is similar to that published in [15] with some distinctions that will be the subject of a separate letter. Note that in the case depicted in Fig. 1 only the regularised IEs corresponding to $m = 1$ are necessary. The features of the latter IEs guarantee the existence and uniqueness of the solution. What is remarkable is that any reasonable discretisation of these IEs yields an algorithm with guaranteed convergence if the order of discretisation is increased.

We have used a Nystrom-type method with Gauss higher-order quadratures, and found that only $5ka\sqrt{\varepsilon}/\pi$ unknowns are needed to compute the far-fields with a uniform relative accuracy of not less than 4 correct digits. This is supported by the plots in Fig. 2, where the dependences of the relative computational errors on the order of discretisation scheme N are presented. These errors are defined as normalised values of the differences between the radiative (and non-radiative) decay rates computed with given N and with $2N$. As one can see, an exponential convergence takes place.

To verify the results, we have also compared them with the data computed using the commercial code FEKO (in [19], it appears that

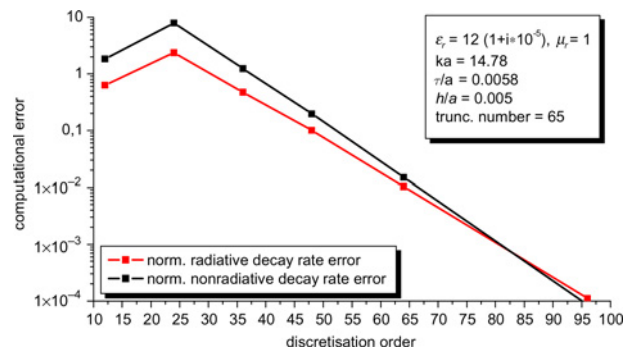


Figure 2 Relative computation errors in terms of the decay components against the order of discretisation scheme. Disk parameters are given in the inset. The truncation number corresponds to the upper limit of integration in the spectral integrals

FEKO uses a boundary IE if applied to the modelling of dielectric scatterers; however, unfortunately, the form of this IE is not disclosed explicitly and the convergence of computations is sometimes questionable), which is based on the planar-surface IEs and the moment-method technique; both sets of data agree well although FEKO needs hours for a single-wavelength computation instead of a few seconds with our method.

Figs. 3 and 4 present, respectively, the dependences of the radiative (P_{rad}) and non-radiative, that is, absorptive (P_{abs}) decay rates on the normalised frequency ka for the dielectric disks with thickness $\tau = 0.0058a$ and permittivity $\varepsilon_r = 12(1 + i\delta)$, where $\delta = 0.2, 0.35, 0.08, 10^{-5}$ correspond to the different losses in the material. If, for instance, the disk diameter is $2a = 5.2 \mu\text{m}$, then $\tau \cong 15 \text{ nm}$ and the largest computed value of $ka = 40$ (conditioned by the requirement that $\tau \ll \lambda$) corresponds to the emission wavelength of 409 nm. The chosen value of dielectric constant corresponds to GaAs in the visible range. Decay rates are normalised by the free-space rate, which is $P_0 = (12\pi)^{-1} Z_0 I^2 (ka)^2$, where I is the dipole current, and $d \ll \lambda$ is the dipole length (see [20], p. 381). One can see the resonances in both the radiative and absorptive decay rates at certain frequencies where the peak values of P_{rad} are several times higher than P_0 . A good insight into the nature of thin-disk resonances can be obtained using the effective index theory [21, 22]. According to this theory, the approximate characteristic equation for the thin-disk resonances of arbitrary azimuthal order m (i.e. with the field dependence given by $\cos m\varphi$) is derived as

$$J_m(\alpha_{\text{eff}}^H ka) \simeq 0 \quad (3)$$

where J_m is the Bessel function of the order m and α_{eff}^H is the

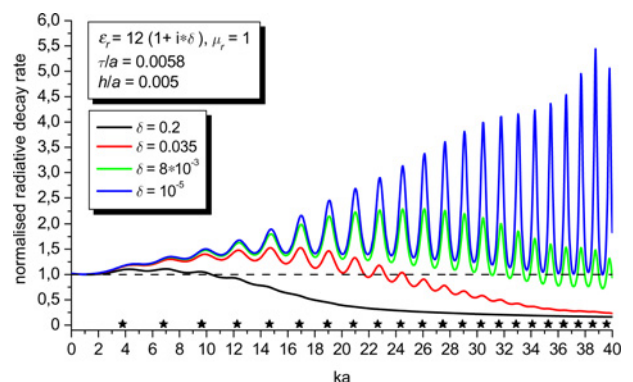


Figure 3 Normalised radiative decay rate against the dimensionless frequency parameter, ka ; the stars indicate the zeros of the approximate characteristic (3) for $m = 1$

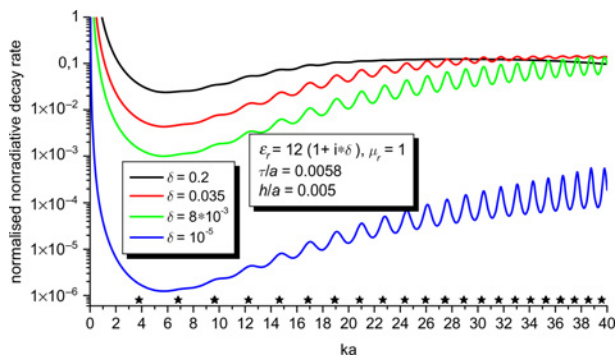


Figure 4 Same as in Fig. 3 for the normalised non-radiative decay rate

effective refractive index of the disk that is smaller than the bulk-material refractive index $\alpha = \sqrt{\epsilon_r}$. The latter quantity is found as the propagation coefficient of the principal TM-polarised natural-guided wave (i.e. having $H_z \neq 0$) of the infinite dielectric layer of the same composition, normalised by the free-space wavenumber. Within the model considered, this value is obtained from the conditions (1) if we use them to find a natural TM-wave guided by a thin material layer. The result is

$$\alpha_{\text{eff}}^H = [1 - 1/(4R^2)]^{1/2} \quad (4)$$

where R is a dimensionless and complex-valued function of the wavelength, layer thickness and dielectric permittivity specified by (2).

In Fig. 5, we have plotted the real and imaginary parts of α_{eff}^H as a function of the normalised frequency, $ka = k\tau(\alpha/\tau)$, for the disk material permittivity $\epsilon_r = 12(1 + i \times 10^{-5})$. As one can see, $\text{Re} \alpha_{\text{eff}}^H > 1 \gg \text{Im} \alpha_{\text{eff}}^H$ in the whole range computed.

In our case of the on-axis EED (Fig. 1), the azimuthal field dependence corresponds to $m = 1$. The roots of (3) for $m = 1$ and $\epsilon = 12$ (i.e. neglecting the losses) are marked with stars in Figs. 3 and 4. They are remarkably close to the corresponding maxima in decay rates, especially in the case of $\delta = 10^{-5}$.

Fig. 6 presents the efficiency η of the radiation, defined as $\eta = P_{\text{rad}}/(P_{\text{rad}} + P_{\text{abs}})$. As one can see, the efficiency displays a broad maximum around $ka \simeq 6$. It drops at lower frequencies because in the static limit the absorbed power decreases less quickly than the radiated power, and also drops down at higher frequencies with the rate conditioned by the bulk losses in the disk material.

Far from the disk, the total field radiated by the EED propagates as an outgoing spherical wave whose complex amplitude depends on the azimuthal and elevation angles. In the configuration studied, the dependence on azimuthal angle is given by the function $\sin \varphi$ or $\cos \varphi$ depending on the field component.

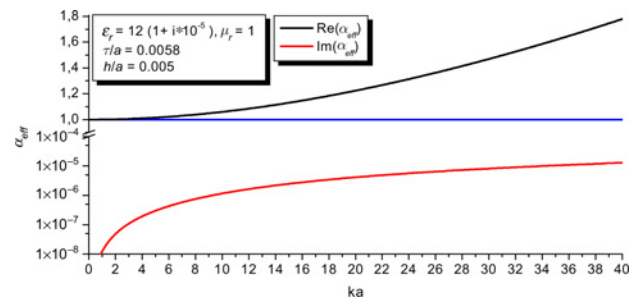


Figure 5 Effective refractive index against ka

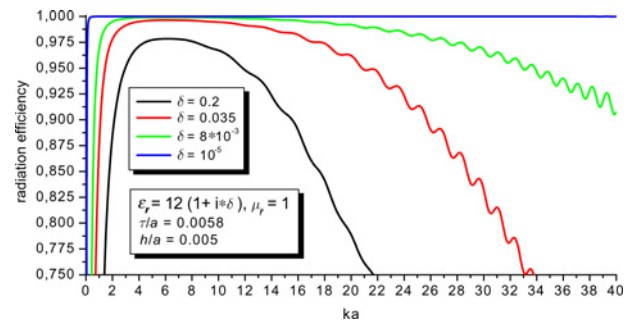


Figure 6 Radiation efficiency against the frequency parameter ka

In Fig. 7, we show the normalised radiation patterns, as a function of the elevation angle, for the Poynting vector of the EED located above a thin dielectric microdisk with $\epsilon_r = 12(1 + i \times 10^{-5})$, for the first three resonances on the plots of Figs. 3 and 4. They demonstrate that at the disk resonances the radiation patterns are dominated by the scattering that occurs predominantly in the disk plane. This is in full agreement with the nature of resonances discussed above as standing cylindrical surface waves formed by the principal-guided TM-wave of a dielectric slab excited by the EED and reflected from the disk rim.

2. Conclusion: In summary, we have accurately quantified the Purcell effect or, equivalently, the modification of spontaneous emission rates (both radiative and absorptive) of the horizontal molecular dipole in the presence of a dielectric microdisk of nanoscale thickness, by studying it from first principles. This has been done over a wide range of the normalised wavelengths: in fact, across the whole visible band if the disk diameter is of several microns. The resonances revealed in the spontaneous emission rates can be explained using the effective refractive index model of the disk. They are caused by the standing waves formed because of the guided wave of the dielectric slab reflection by the disk rim. This

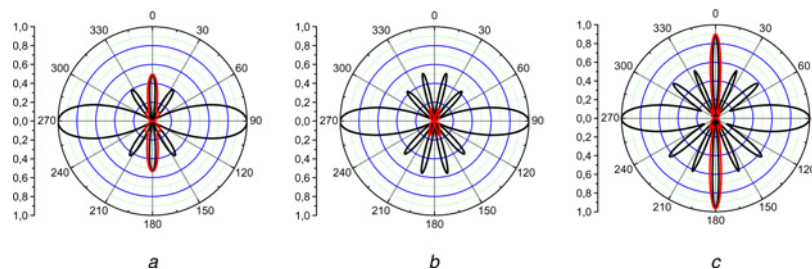


Figure 7 Normalised radiation patterns for the disk with $\epsilon_r = 12(1 + i \times 10^{-5})$ in the resonances at $ka = 12.42$
a $ka = 14.78$
b $ka = 17.02$
c In two planes: $\varphi = 0$ (red) and $\varphi = \pi/2$ (black)

observation can serve as a de-facto justification of this empirical model from the viewpoint of rigorous Maxwell theory.

Following [15], the same method can be also used for the accurate analysis of the spontaneous emission of an arbitrarily located and oriented molecular dipole in the presence of a thin microdisk. Such a general case analysis, however, requires the solution of a sufficient number of independent pairs of the coupled regularised IEs corresponding to different azimuthal orders m ; therefore this analysis will be presented as a full-size paper elsewhere. Thus, the analytical–numerical method that has been applied here places thin material disks in the same position as spherical scatterers in the sense that they can be computed very economically and with controlled accuracy.

3. Acknowledgment: This work was supported by the National Academy of Sciences of Ukraine via the State Target Program ‘Nanotechnologies and Nanomaterials,’ and the European Science Foundation via the Networking Programme ‘Newfocus.’

4 References

- [1] Vuckovic J., Painter O., Xu Y., Yariv A., Scherer A.: ‘Finite-difference time-domain calculation of the spontaneous emission coupling factor in optical microcavities’, *IEEE J. Quantum Electron.*, 1999, **35**, (8), pp. 1168–1175
- [2] Xu Y., Lee R.K., Yariv A.: ‘Finite-difference time-domain analysis of spontaneous emission in a microdisk cavity’, *Phys. Rev. A*, 2000, **61**, (3), p. 033808
- [3] Rogobete L., Henkel C.: ‘Spontaneous emission in a subwavelength environment characterized by boundary integral equations’, *Phys. Rev. A*, 2004, **70**, p. 063815
- [4] Rogobete L., Kaminski F., Agio M., Sandoghdar V.: ‘Design of plasmonic nanoantennae for enhancing spontaneous emission’, *Opt. Lett.*, 2007, **32**, (12), pp. 1623–1625
- [5] Ding W., Bachelot R., Espiau de Lamaestre R., Macias D., Baudrion A.-L., Royer P.: ‘Understanding near/far-field engineering of optical dimer antennas through geometry modification’, *Opt. Express*, 2009, **17**, (23), pp. 21228–21239
- [6] Biagioni P., Huang J.S., Duò L., Finazzi M., Hecht B.: ‘Cross resonant optical antenna’, *Phys. Rev. Lett.*, 2009, **102**, (25), p. 256801
- [7] Koenderink A.F.: ‘On the use of Purcell factors for plasmon antennas’, *Opt. Lett.*, 2010, **35**, (24), pp. 4208–4210
- [8] Xu Y.: ‘Electromagnetic scattering by an aggregate of spheres’, *Appl. Opt.*, 1995, **34**, (1), pp. 4573–4588
- [9] Boriskin A.V., Boriskina S.V., Rolland A., Sauleau R., Nosich A.I.: ‘Test of the FDTD accuracy in the analysis of the scattering resonances associated with high-Q whispering-gallery modes of a circular cylinder’, *J. Opt. Soc. Am. A*, 2008, **25**, (5), pp. 1169–1173
- [10] Niegemann J., Pernice W., Busch K.: ‘Simulation of optical resonators using DGT and FDTD’, *J. Pure Appl. Opt. A*, 2009, **11**, (11), pp. 4015–4024
- [11] Søndergaard T., Tromborg B.: ‘Lippmann–Schwinger integral equation approach to the emission of radiation by sources located inside finite-sized dielectric cylinders’, *Phys. Rev. E*, 2002, **66**, (155309), pp. 1–13
- [12] Wilton D.: ‘Review of current status and trends in the use of integral equations in computational electromagnetics’, *Electromagnetics*, 1992, **12**, (3–4), pp. 287–341
- [13] Muller C.: ‘Foundations of the mathematical theory of electromagnetic waves’ (Springer-Verlag, Berlin, 1969)
- [14] Nosich A.I., Smotrova E.I., Boriskina S.V., Benson T.M., Sewell P.: ‘Trends in microdisk laser research and linear optical modelling’, *Opt. Quantum Electron.*, 2007, **39**, (15), pp. 1253–1272
- [15] Balaban M.V., Sauleau R., Benson T.M., Nosich A.I.: ‘Dual integral equations technique in electromagnetic wave scattering by a thin disk’, *Prog. Electromagn. Res. B*, 2009, **16**, pp. 107–126
- [16] Bleszynski E., Bleszynski E., Jaroszewicz T.: ‘Surface-integral equations for electromagnetic scattering from impenetrable and penetrable sheets’, *IEEE Antennas Propag. Mag.*, 1993, **36**, (6), pp. 14–24
- [17] Zinenko T.L., Nosich A.I., Okuno Y.: ‘Plane wave scattering and absorption by resistive-strip and dielectric-strip periodic gratings’, *IEEE Trans. Antennas Propag.*, 1998, **46**, (10), pp. 1498–1505
- [18] Nosich A.I.: ‘Method of analytical regularization in wave-scattering and eigenvalue problems: foundations and review of solutions’, *IEEE Antennas Propag. Mag.*, 1999, **42**, (3), pp. 34–49
- [19] <http://www.feko.info>
- [20] Rothwell E.J., Cloud M.J.: ‘Electromagnetics’ (CRC Press, Boca Raton, 2009, 2nd edn.)
- [21] Slusher R.E., Levi A.F.J., Mohideen U., McCall S.L., Pearton S.J., Logan R.A.: ‘Threshold characteristics of semiconductor microdisk lasers’, *Appl. Phys. Lett.*, 1993, **63**, (10), pp. 1310–1312
- [22] Smotrova E.I., Nosich A.I., Benson T.M., Sewell P.: ‘Cold-cavity thresholds of microdisks with uniform and non-uniform gain: quasi-3D modeling with accurate 2D analysis’, *IEEE J. Sel. Top. Quantum Electron.*, 2005, **11**, (5), pp. 1135–1142